Supporting Information

for

Liquid Phase Multicomponent Adsorption and Separation of Xylene Mixtures by Flexible MIL-53 Adsorbents

Mayank Agrawal[1,‡], Souryadeep Bhattacharyya[1,‡], Yi Huang[1,‡], Krishna C. Jayachandrababu[1,‡], Christopher R. Murdock, Jason A. Bentley[1], Alejandra Rivas-Cardona[2], Machteld M. Mertens[2], Krista S. Walton[1,*], David S. Sholl[1,*], and Sankar Nair[1,*]

[1]*School of Chemical & Biomolecular Engineering, Georgia Institute of Technology, Atlanta, GA 30332-0100, USA*

[2]*ExxonMobil Chemical Company, Baytown, TX 77520, USA*

[‡]These authors contributed equally

*Corresponding authors: sankar.nair@chbe.gatech.edu, david.sholl@chbe.gatech.edu; krista.walton@chbe.gatech.edu

Table S1. Recipes and conditions for MIL-53 synthesis.

Materials	**Molar Ratio of Added Reagents in a 45-mL Teflon Cup**	**Synthesis Condition**
MIL-53(Al)	80 H_2O (20 g):1 $AlCl_3 \cdot 6H_2O$ (3.35 g):0.5 BDC (1.152 g)	493 K/72 h
MIL-53(Cr)	100 H_2O (18 g):1 $CrCl_3 \cdot 6H_2O$ (2.776 g):1 BDC (1.695 g)	483 K/12 h
MIL-53(Ga)	285 H_2O (20 g):1 $Ga(NO_3)_3 \cdot xH_2O$ (1 g):1.2 BDC (0.76 g)	483 K/4 h
MIL-53(Fe)	28.4 DMF (18.88 g):1 $FeCl_3 \cdot 6H_2O$ (1.081 g):1 BDC (0.665 g)	423 K/24 h
MIL-53(Sc)	300 DMF (20.25 g) :15 Pyridine (1.099 g): 1 $Sc(NO_3)_3 \cdot xH_2O$ (0.856 g):1 BDC (0.616 g)	463 K/40 h

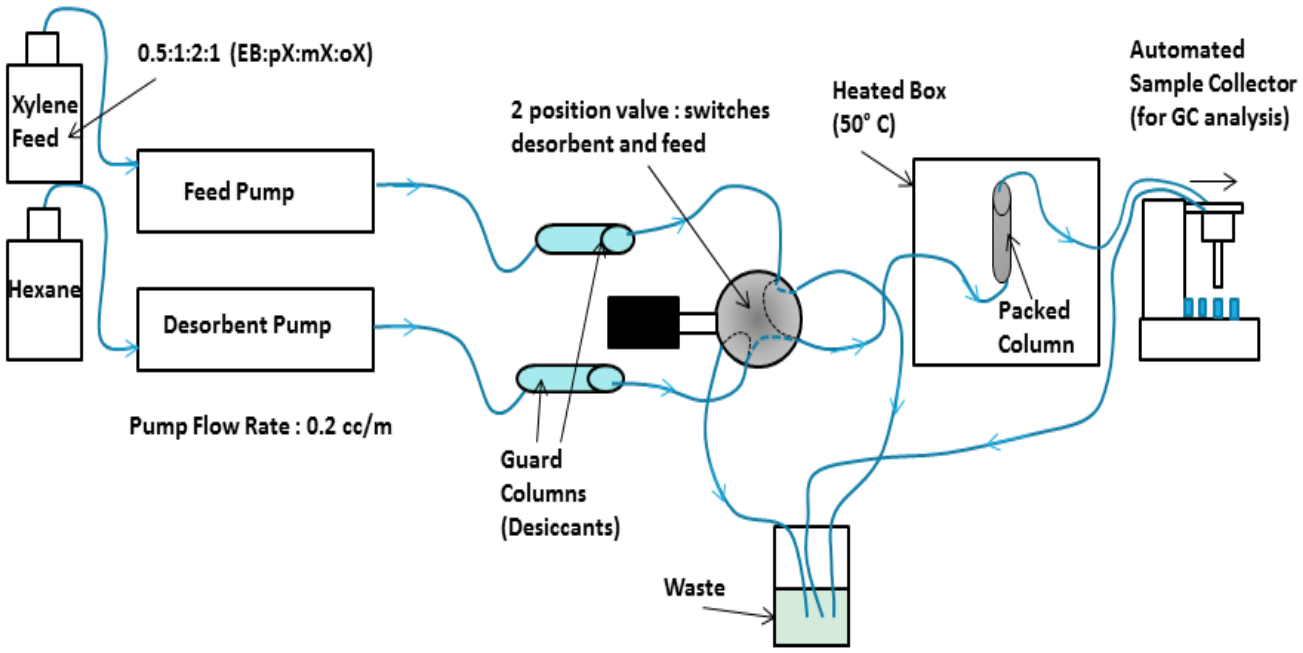

Figure S1. Schematic of the liquid breakthrough setup used in multicomponent liquid breakthrough experiments.

Additional OFAST Simulation Details

The osmotic framework adsorption solution theory (OFAST) method[1-2] was used to describe structural transition of MIL-53 due to C_8 aromatics adsorption. In the method, the osmotic potential, Ω, is calculated for adsorption of any adsorbates for metastable host rigid frameworks. System having the lowest osmotic potential at a given set of conditions is favored to be at equilibrium by thermodynamics. Here, we have considered only single component adsorption, for which Ω is defined as:

$$\Omega_k(T,f) = F^k_{host}(T) + PV_k - RT\int_0^f \frac{n^e_k(f,T)}{f}df \quad \text{(S1)}$$

Here F_{host} is the Helmholtz free energy of the empty framework, n^{e} is the excess amount of adsorbate molecules adsorbed in the framework, and f is the fugacity of the bulk fluid phase. At low pressures, the excess adsorbed amount is equal to absolute adsorbed amount and the fugacity is equal to the pressure. For two pore structures in MIL-53, Equation S1 becomes:

$$\Delta G_{total} = \Delta\Omega_{total} = \Delta F_{host} + P\Delta V - RT\int_0^f \frac{\Delta n^e}{f}df \quad \text{(S2)}$$

At a transition pressure, at which one structure makes a transition to another structure, Equation S2 becomes equal to zero as both structures have same osmotic potential at that pressure. So, if we have free energy difference between both structures, transition pressure can be calculated and vice versa. It is difficult to accurately calculate free energy differences between frameworks at a particular temperature. So, we used transition pressure of one adsorbate from the experiments (oX in this paper) to calculate free energy difference of narrow pore and large pore frameworks, and then used that free energy difference to calculate transition pressures for other C_8 aromatics in single component adsorption. Because the narrow-pore structures show no adsorption in our

calculations, this transition pressures is same as the pressure at which adsorbate loading starts in the isotherms.

Force Field Parameters for MD calculations

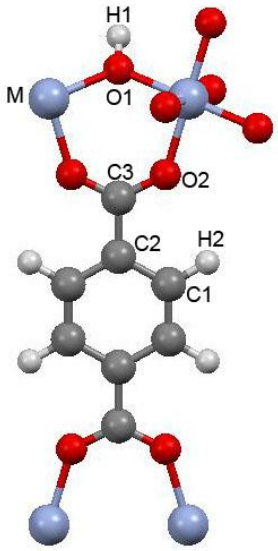

Figure S2. Atomic configuration of MIL-53 with atom types labeled. Here, M = Cr, Al, Ga, Fe.

Table S2. Lennard Jones parameters for framework atoms.

Atom Type	**ε_{ii} (kJ/mol)**	**σ_{ii} (Å)**
C	0.2478	3.81
H	0.1602	2.45
O	0.2495	3.12
Cr	0.0627	2.69
Al	1.2955	3.91
Ga	1.7343	3.91
Fe	0.0543	2.59

Note: These parameters are taken from the force field for MIL-53(Cr)[3] derived by Ma et al. Parameters for Al, Ga and Fe are taken from UFF.[4]

Table S3. DDEC charges for frameworks.

Atom Type	MIL-53(Cr)	MIL-53(Al)	MIL-53(Ga)	MIL-53(Fe)
C1	-0.0789	-0.0732	-0.0763	-0.0779
C2	-0.0946	-0.1042	-0.0937	-0.0868
C3	0.6804	0.7342	0.7133	0.6470
O1	-0.9432	-1.0993	-1.0004	-0.7279
O2	-0.6099	-0.6479	-0.6251	-0.5143
H1	0.4644	0.4788	0.4691	0.4374
H2	0.1113	0.1120	0.1138	0.1093
Cr	1.6172	-	-	-
Al	-	1.7969	-	-
Ga	-	-	1.6425	-
Fe	-	-	-	1.1016

Note: These values are derived using *ab initio* calculations.

Table S4. Bond stretch parameters for MIL-53.

i-j	k_{ij} [kJ/(mol.Å^2)]	r_0 (Å)
C1-C1	4015.05	1.34
C1-C2	4015.05	1.34
C2-C3	2943.72	1.47
C3-O2	4516.93	1.25
C1-H2	2850.14	1.09
O1-Cr	2041.72	1.95
O2-Cr	2041.72	1.95
O1-Al	1830.24	1.93
O2-Al	1830.24	1.93
O1-Ga	1755.99	2.02
O2-Ga	1755.99	2.02
O1-Fe	2109.65	1.93
O2-Fe	2109.65	1.93

The flexible force fields for MIL-53 have been derived starting with those previously reported for MIL-53(Cr) Ma *et al.*[3] In this force field, the intramolecular force constant for organic moiety were extracted from the widely used Consistent Valence Force Field (CVFF)[5] same as for the inorganic part. For metal-oxygen intramolecular and non-bonded interactions parameters were adopted from UFF[4, 6] force field. C3-O2-M(metal) three body interactions were considered to have the same values for all metals. The torsion terms are adjusted to reproduce basic structural features of MIL-53 frameworks. Note that the non-bonded interactions concern atoms separated by exactly three bonds usually described as 1-4 van der Waals interactions with LJ potentials.

Table S5. Bond bending parameters for MIL-53.

i-j-k	k_{ij} [kJ/(mol.rad^2)]	Θ (^{0})
C1-C2-C1	753.30	120
C1-C1-C2	753.30	120
C1-C1-H2	309.72	120
C2-C1-H2	309.72	120
C1-C2-C3	290.32	120
C2-C3-O2	569.25	120
O2-C3-O2	114.16	123
C3-O2-Cr	115.9	136
C3-O2-Al	115.9	136
C3-O2-Ga	115.9	136
C3-O2-Fe	115.9	136

Table S6. Torsional parameters for MIL-53.

i-j-k-l	k_{ij} [kJ/(mol.rad^2)]	N	Θ (^{0})
C2-C1-C1-C2	2.0	2	180
C3-C2-C1-C1	2.0	2	180
C2-C1-C1-H2	2.0	2	180
H2-C1-C1-H2	2.0	2	180
C3-C2-C1-H2	2.0	2	180
H2-C1-C2-C1	2.0	2	180
C1-C1-C2-C1	2.0	2	180
C1-C2-C3-O2	5.0	2	180
C2-C3-O2-Cr	20.0	2	180
C2-C3-O2-Al	18.0	2	180
C2-C3-O2-Ga	22.0	2	180
C2-C3-O2-Fe	22.0	2	180

Table S7. DFT-optimized lattice parameters for MIL-53 materials.

	a (Å)	b (Å)	c (Å)	a (Å)	b (Å)	c (Å)
	DFT Simulations			Experiments[7-9]		
MIL-53(Cr)						
Large pore (LP)	16.73	13.29	6.74	16.77	13.03	6.81
MIL-53(Cr)						
Narrow pore (NP)	19.85	6.20	6.51	19.68	7.84	6.78
NP_water loaded	19.62	7.76	6.62			
MIL-53(Al)						
Large pore	16.64	13.42	6.76	16.67	13.33	6.80
MIL-53(Al)						
Narrow pore	19.75	6.26	6.62	19.79	7.94	6.81
NP_waterloaded	19.68	7.83	6.68			
MIL-53(Ga)						
Large pore	16.93	13.12	6.76	16.85	13.01	6.82
MIL-53(Ga)						
Narrow pore	19.89	6.12	6.82	19.81	7.96	6.80
NP_waterloaded	19.78	7.72	6.86			
MIL-53(Fe)						
Large pore	16.67	13.20	6.60	16.89	12.54	6.58
MIL-53(Fe)						
Narrow pore	19.54	6.24	6.35	19.51	7.61	6.57
NP_waterloaded	19.44	7.65	6.63			

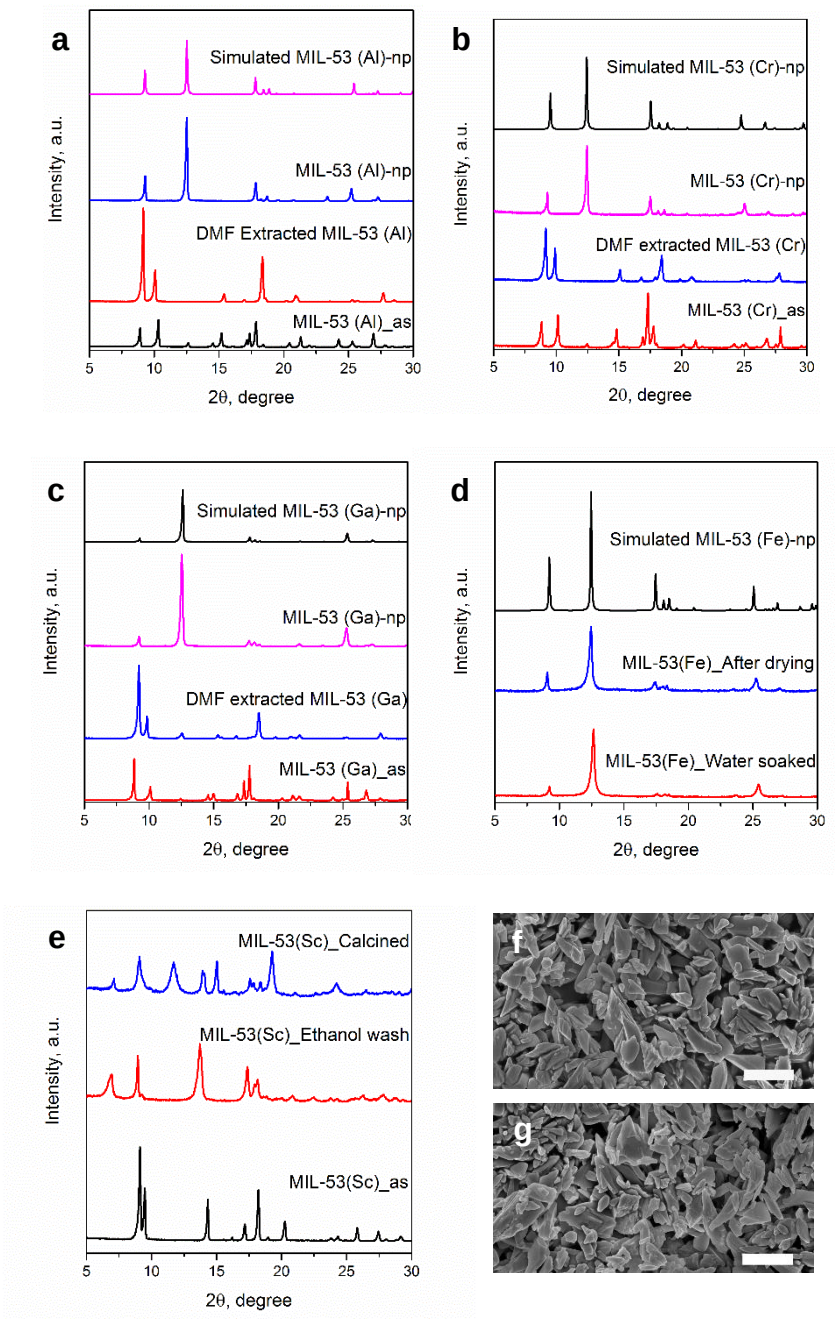

Figure S3. Powder-XRD patterns (a)-(e) and SEM images (f)-(g) of MIL-53 adsorbents at different stage of synthesis. (a) MIL-53 (Al), (b) MIL-53 (Cr), (c) MIL-53 (Ga), (d) MIL-53 (Fe), (e) MIL-53 (Sc), (f) washed MIL-53 (Sc), and (g) calcined MIL-53 (Sc). Impure peak at 2θ angle of ~ 17.3° in (a)~(e) was ascribed to the excess BDC linkers in the as-synthesized (as) sample. Scale bars in (f-g) are 2 µm.

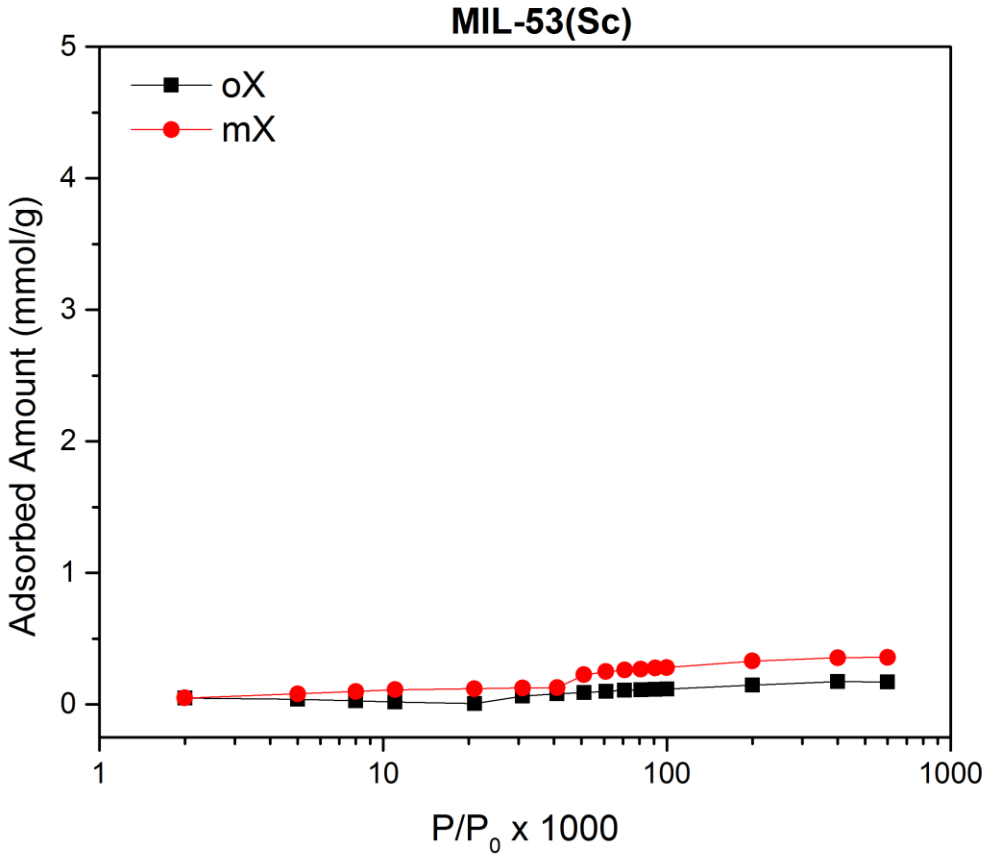

Figure S4. Adsorption isotherms of mX and oX on MIL-53(Sc) at 323 K.

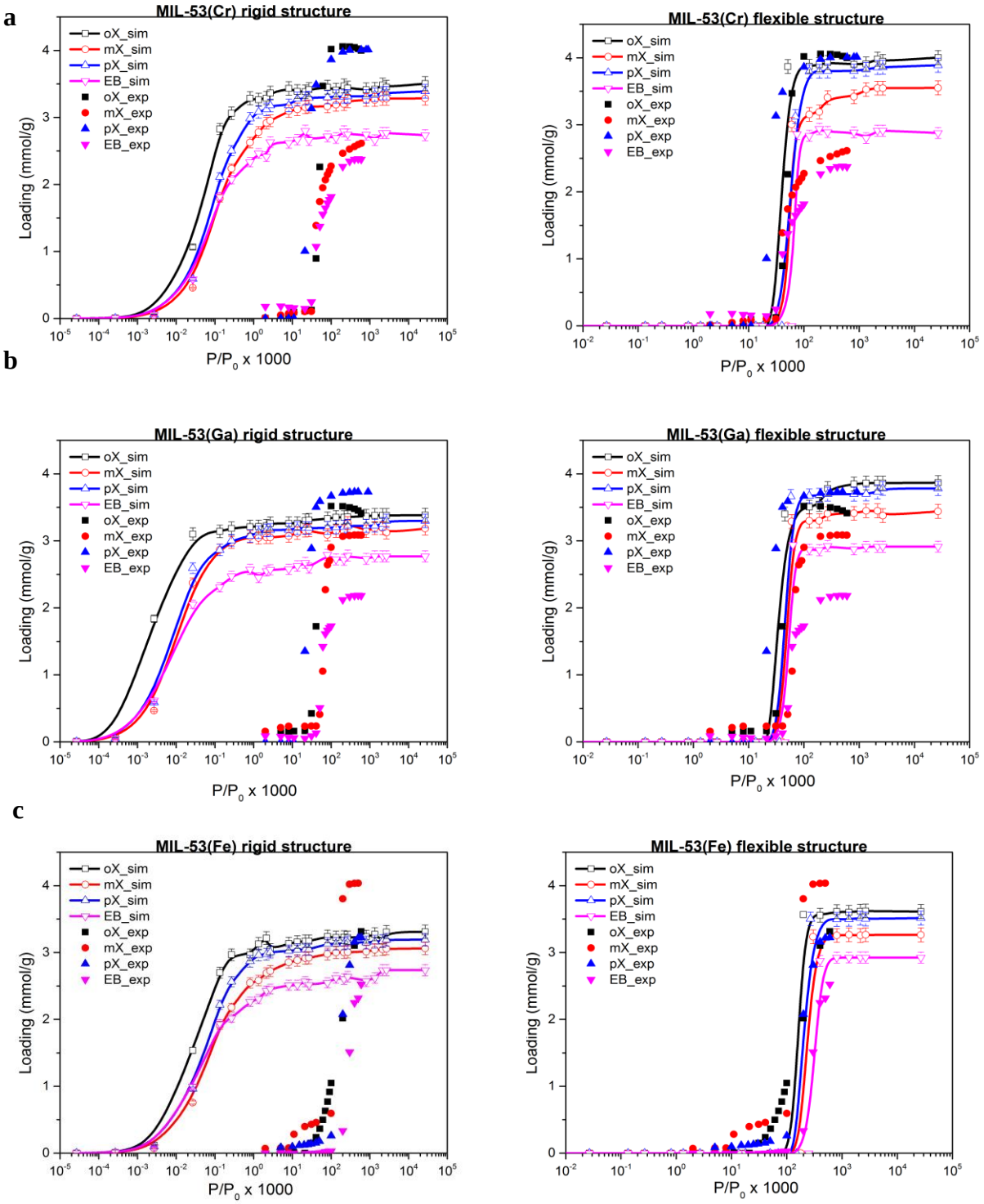

Figure S5. Rigid-structure and flexible-structure simulations compared with experimental data for single-component adsorption of xylene isomers in (a) MIL-53(Cr), (b) MIL-53(Ga) and (c) MIL-53(Fe).

Table S8. Summary comparison of experimental and simulated unary adsorption characteristics of C_8 aromatics in MIL-53 materials. The error bars on the data are approximately 0.1 mmol/g.

Material	**Single-component saturation capacity (mmol/g)**			
	oX	**pX**	**mX**	**EB**
MIL-53(Al)				
Experiment	4.5	4.6	4.5	2.5
Simulation	4.4	4.3	4.0	3.3
MIL-53(Cr)				
Experiment	4.0	4.2	2.6	2.4
Simulation	3.9	3.8	3.6	2.9
MIL-53(Ga)				
Experiment	3.4	3.7	3.1	2.2
Simulation	3.8	3.75	3.5	2.9
MIL-53(Fe)				
Experiment	3.3	4.0	3.2	2.5
Simulation	3.7	3.6	3.3	2.8

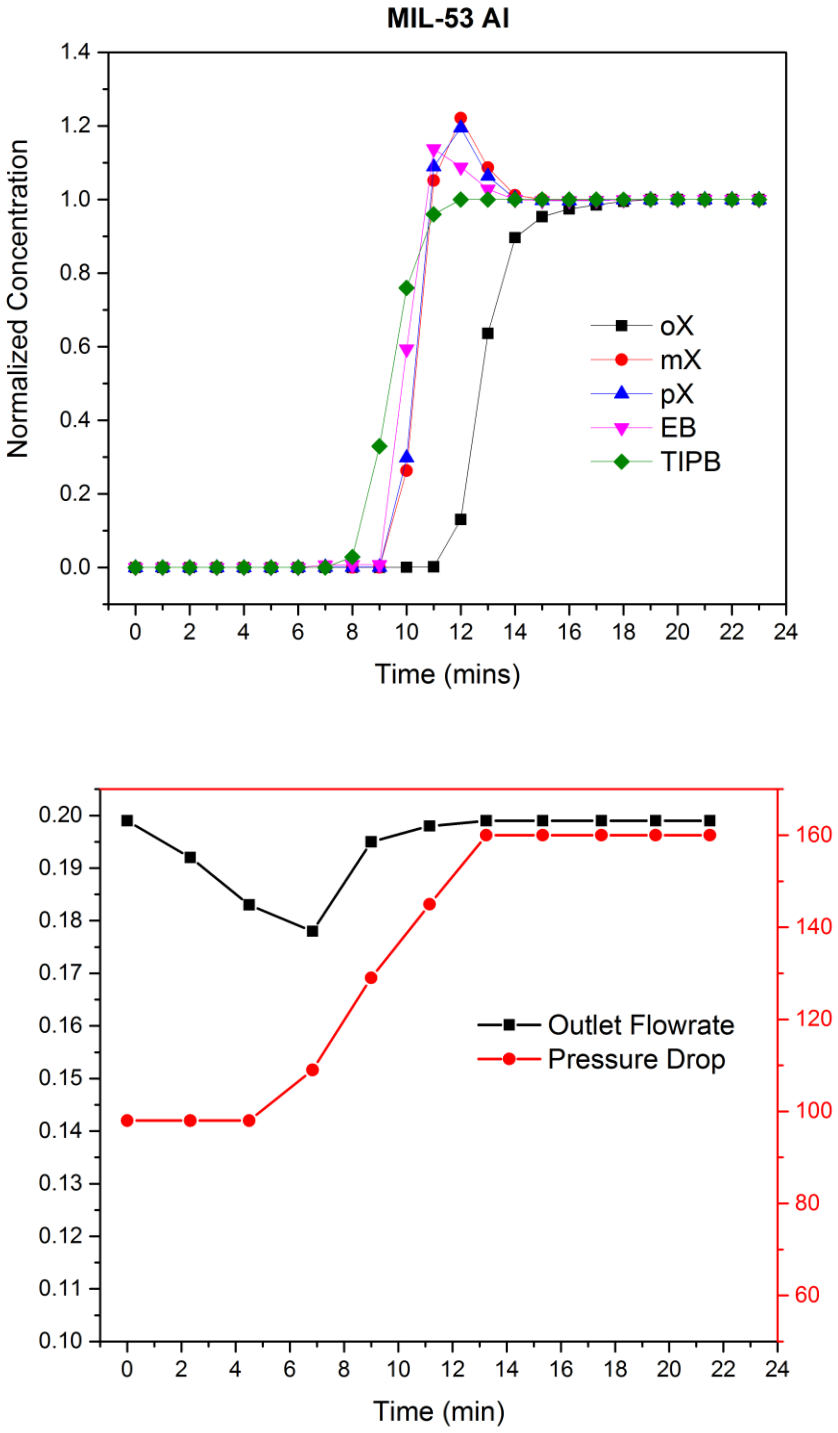

Figure S6. Variation of outlet flowrate and pressure drop observed across a MIL-53(Al) column during breakthrough of a 0.5:1:2:1 EB:pX:mX:oX feed mixture at 100 psi backpressure and 323 K. The data shown in the top panel is the same as **Figure 4a**.

Table S9. Comparison of computational and experimental adsorption capacity and selectivity values for different MIL-53 adsorbents under quaternary liquid-phase adsorption with a 0.5:1:2:1 EB:pX:mX:oX mixture at 323 K and 100 psi.

	Capacity (mmol/g)					Selectivity				
Material	**oX**	**mX**	**pX**	**EB**	**Total**	**oX/oX**	**oX/mX**	**oX/pX**	**oX/EB**	**oX/All**
MIL-53(Cr)										
Simulations	1.7±0.2	1.4±0.1	0.6±0.1	0.3±0.02	3.9±0.2	1.0	2.4±0.3	2.7±0.2	3.3±0.2	2.6±0.3
Experiments	2.5±0.2	1.6±0.1	0.6±0.1	0.25±0.04	4.9±0.2	1.0	2.8±0.4	3.7±0.6	4.9 ±1	3.2±0.5
MIL-53(Al)										
Simulations	2.0±0.2	1.5±0.2	0.7±0.1	0.3±0.03	4.5±0.2	1.0	2.8±0.4	2.9 ±0.3	3.6±0.2	3±0.3
Experiments	3±0.1	1±0.2	0.49±0.1	0.14±0.04	4.6±0.3	1.0	5.1±0.9	5.2±1	8.2±2	5.5±1
MIL53(Ga)										
Simulations	1.6±0.2	1.3±0.1	0.6±0.1	0.2±0.03	3.7±0.2	1.0	2.6±0.3	2.9±0.2	3.4±0.2	2.7±0.3
Experiments	1.5±0.1	1.2±0.1	0.47±0.1	0.18±0.06	3.4±0.2	1.0	2.5±0.2	3.3±0.3	4.7±0.5	2.9±0.2

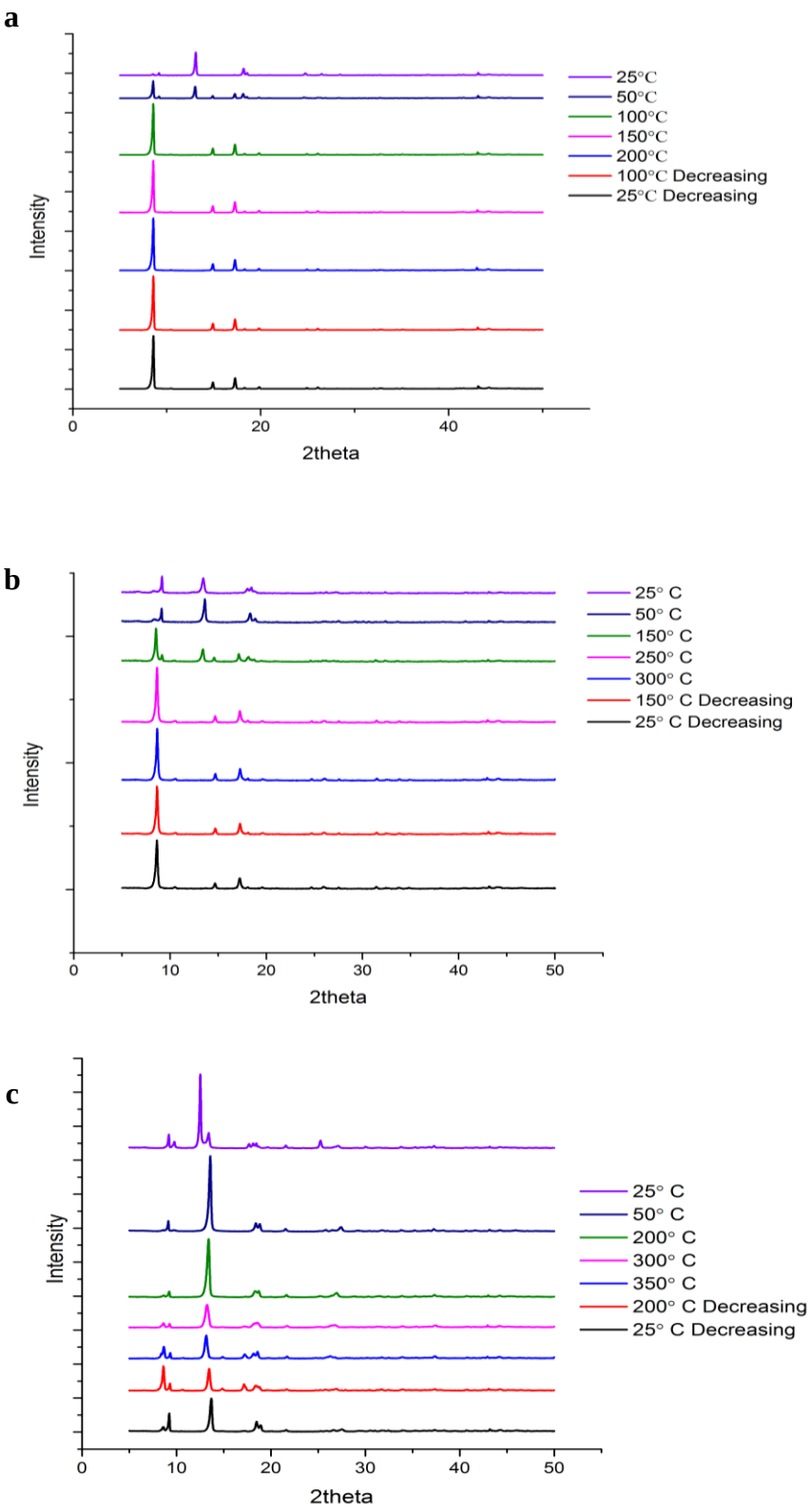

Figure S7. Temperature-dependent PXRD patterns under nitrogen flow, for (a) Mil-53(Al), (b) Mil-53(Cr) and (c) Mil-53(Ga). The patterns are vertically offset for ease of display.

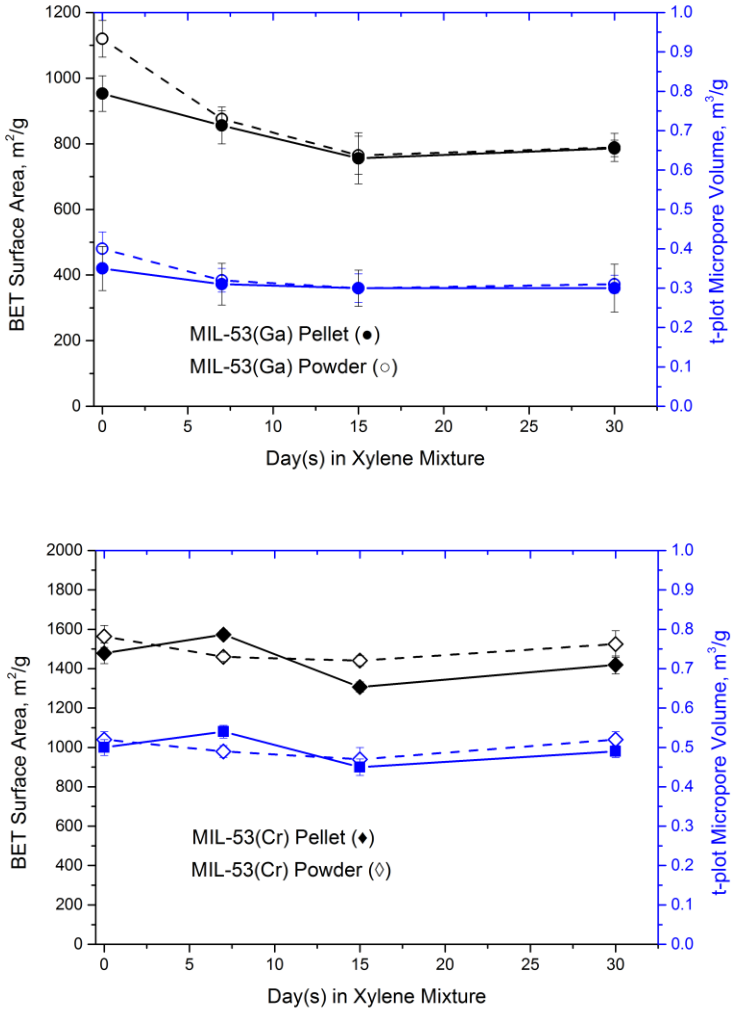

Figure S8. BET surface area of MIL-53(Ga) and MIL-53(Cr) powders and pellets immersed in 0.5:1:2:1 EB:pX:mX:oX mixture at 323 K for periods up to 30 days.

Table S10. Textural properties of MIL-53 powders and pellets after immersion in a 0.5:1:2:1 EB:pX:mX:oX mixture for 30 days at 323 K. The numbers (0,7,15, 30) in the sample names denote the number of days of immersion. The numbers in parentheses are standard deviations calculated based on three independent measurements of each sample.

MIL-53(Al) Samples	BET Area m^2/g	Pore Volume m^3/g
powder_0	1706 (102)	0.60 (0.01)
powder_7	1747 (56)	0.60 (0.02)
powder_15	1432 (75)	0.44 (0.04)
powder_30	1477 (35)	0.46 (0.05)
Pellet_0	1707 (65)	0.60 (0.02)
pellet_7	1412 (25)	0.50 (0.02)
pellet_15	1357 (65)	0.48 (0.03)
pellet_30	1516 (95)	0.54 (0.03)

MIL-53(Cr) Samples	BET Area m^2/g	Pore Volume m^3/g
powder_0	1564 (56)	0.52 (0.02)
powder_7	1460 (23)	0.49 (0.01)
powder_15	1441 (25)	0.47 (0.03)
powder_30	1525 (68)	0.52 (0.02)
pellet_0	1478 (52)	0.50 (0.02)
pellet_7	1573 (26)	0.54 (0.02)
pellet_15	1307 (23)	0.45 (0.02)
pellet_30	1419 (46)	0.49 (0.01)

MIL-53(Ga) Samples	BET Area m^2/g	Pore Volume m^3/g
powder_0	1120 (55)	0.40 (0.04)
powder_7	876 (25)	0.32 (0.03)
powder_15	765 (58)	0.30 (0.03)
powder_30	789 (43)	0.31 (0.02)
pellet_0	953 (54)	0.35 (0.05)
pellet_7	856 (56)	0.31 (0.05)
pellet_15	756 (78)	0.30 (0.04)
pellet_30	786 (25)	0.30 (0.06)

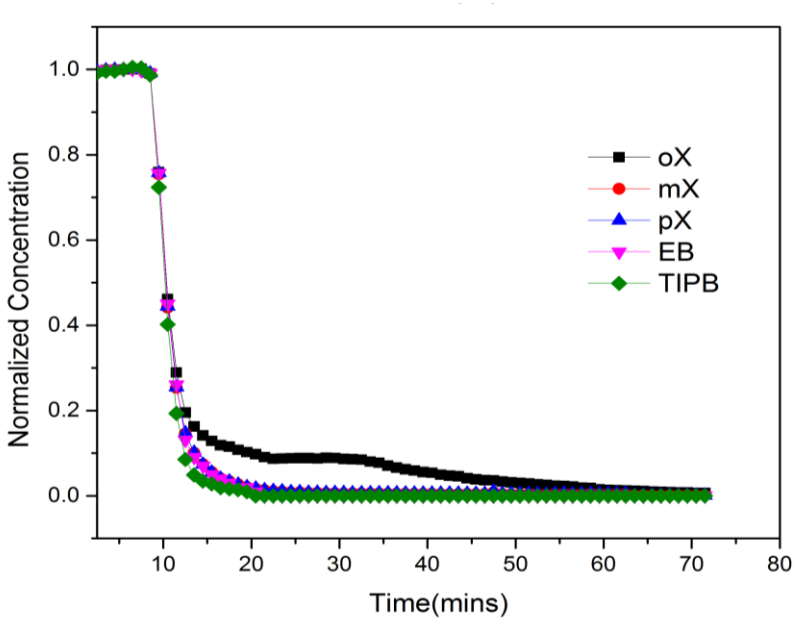

Figure S9. Desorption trace of adsorbed aromatic isomers in a MIL-53(Al) column using a hexane desorbent, following a breakthrough adsorption run with feed mixture 0.5:1:2:1 EB:pX:mX:oX at 100 psi and 323 K.

Table S11. Calculated experimental desorption selectivity values for MIL-53(Al) adsorbent after a quaternary liquid-phase breakthrough run with a 0.5:1:2:1 EB:pX:mX:oX mixture using hexane as desorbent at a flowrate of 0.2 cc/min at 323 K and 100 psi.

oX/pX	5.3
oX/mX	5.3
oX/EB	9.4

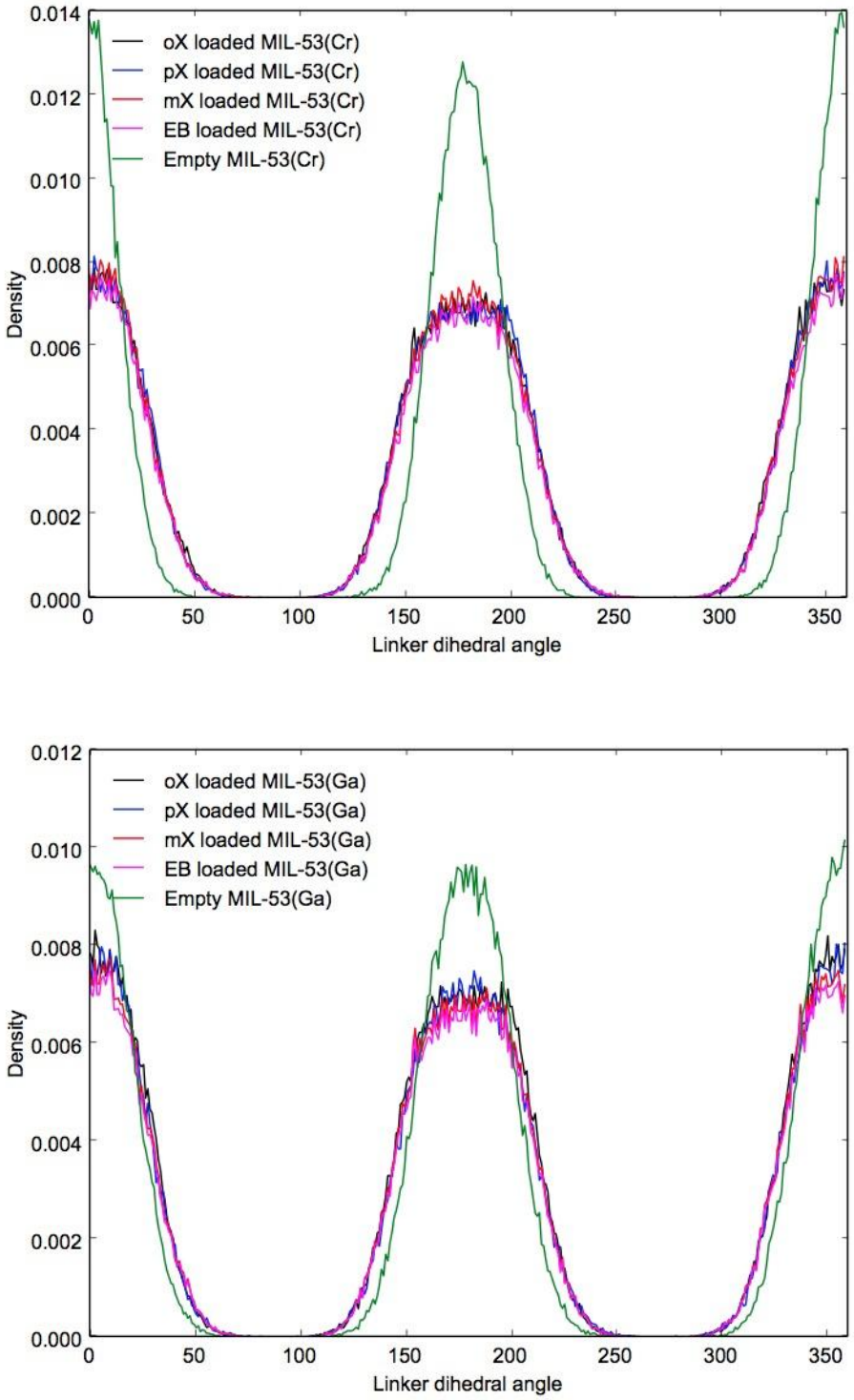

Figure S10. Calculated distribution of linker dihedral angles in MIL-53(Cr) and MIL-53(Ga).

Supporting References

1. Coudert, F. X. The Osmotic Framework Adsorbed Solution Theory: Predicting Mixture Coadsorption in Flexible Nanoporous Materials. *Phys. Chem. Chem. Phys.* **2010**, *12*, 10904-10913.

2. Zhang, C.; Gee, J. A.; Sholl, D. S.; Lively, R. P. Crystal-Size-Dependent Structural Transitions in Nanoporous Crystals: Adsorption-Induced Transitions in ZIF-8. *J. Phys. Chem. C* **2014**, *118*, 20727-20733.

3. Ma, Q.; Yang, Q.; Ghoufi, A.; Ferey, G.; Zhong, C.; Maurin, G. Guest Dependent Pressure Behavior of the Flexible MIL-53(Cr): A Computational Exploration. *Dalton Trans.* **2012**, *41*, 3915-3919.

4. Rappe, A. K.; Casewit, C. J.; Colwell, K. S.; Goddard, W. A.; Skiff, W. M. UFF, A Full Periodic Table Force Field for Molecular Mechanics and Molecular Dynamics Simulations. *J. Am. Chem. Soc.* **1992**, *114*, 10024-10035.

5. Dauberosguthorpe, P.; Roberts, V. A.; Osguthorpe, D. J.; Wolff, J.; Genest, M.; Hagler, A. T. Structure and Energetics of Ligane-Binding to Proteins-Escherichia-Coli Dihydrofolate Reductase Trimethoprim, A Drug-Receptor System. *Proteins* **1988**, *4*, 31-47.

6. Mayo, S. L.; Olafson, B. D.; Goddard, W. A. DREIDING: A Generic Force Field for Molecular Simulations. *J. Phys. Chem.* **1990**, *94*, 8897-8909.

7. Serre, C.; Millange, F.; Thouvenot, C.; Nogue`s, M.; Marsolier, G. r.; Loue¨r, D.; Fe´rey, G. r. Very Large Breathing Effect in the First Nanoporous Chromium(III)-Based Solids: MIL-53 or $Cr^{III}(OH)\cdot\{O_2C{-}C_6H_4{-}CO_2\}\cdot\{HO_2C{-}C_6H_4{-}CO_2H\}_x\cdot H_2O_y$. *J. Am. Chem. Soc.* **2002**, *124*, 13159-13526.

8. Biswas, S., et al. New Functionalized Metal–Organic Frameworks MIL-47-X (X = −Cl, −Br, $-CH_3$, $-CF_3$, −OH, $-OCH_3$): Synthesis, Characterization, and CO_2 Adsorption Properties. *J. Phys. Chem. C* **2013**, *117*, 22784-22796.

9. Ahnfeldt, T.; Gunzelmann, D.; Loiseau, T.; Hirsemann, D.; Senker, J.; Ferey, G.; Stock, N. Synthesis and Modification of a Functionalized 3D Open-Framework Structure with MIL-53 Topology. *Inorg. Chem.* **2009**, *48*, 3057-3064.